JACS
JOURNAL OF THE AMERICAN CHEMICAL SOCIETY

Article

pubs.acs.org/JACS

Spectroscopic and Computational Insights on Catalytic Synergy in Bimetallic Aluminophosphate Catalysts

Matthew E. Potter,*[,†,‡] A. James Paterson,[‡] Bhoopesh Mishra,[§] Shelly D. Kelly,[∥] Simon R. Bare,[∥] Furio Corà,[⊥] Alan B. Levy,[#] and Robert Raja*[,‡]

[†]Department of Chemical and Biochemical Engineering, Georgia Institute of Technology, 311 Ferst Drive, Atlanta, Georgia 30332, United States

[‡]School of Chemistry, University of Southampton, Southampton, Hampshire SO17 1BJ, United Kingdom

[§]Physics Department, Illinois Institute of Technology, Chicago, Illinois 60016, United States

[∥]UOP LLC, A Honeywell Company, 25 East Algonquin Road, Des Plaines, Illinois 60017, United States

[⊥]Department of Chemistry, University College London, 20 Gordon Street, London WC1H 0AJ, U.K.

[#]Honeywell International, 101 Columbia Road, Morristown, New Jersey 07962, United States

Supporting Information

ABSTRACT: A combined electronic structure computational and X-ray absorption spectroscopy study was used to investigate the nature of the active sites responsible for catalytic synergy in Co−Ti bimetallic nanoporous frameworks. Probing the nature of the molecular species at the atomic level has led to the identification of a unique Co−O−Ti bond, which serves as the loci for the superior performance of the bimetallic catalyst, when compared with its analogous monometallic counterpart. The structural and spectroscopic features associated with this active site have been characterized and contrasted, with a view to affording structure−property relationships, in the wider context of designing sustainable catalytic oxidations with porous solids.

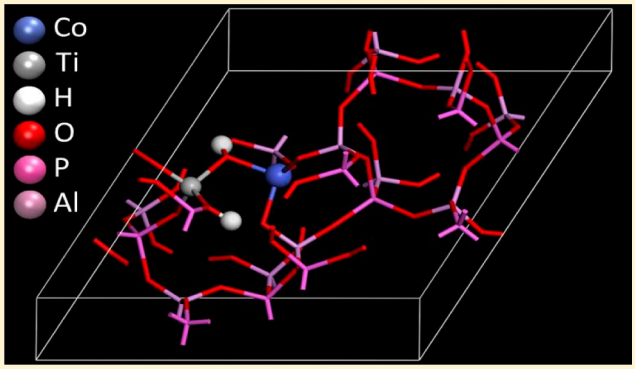

INTRODUCTION

Growing global concerns over greenhouse gas emissions and finite energy resources have facilitated growth in many areas of materials science. Catalysis is no exception. The desire for cheaper, cleaner, and more efficient technologies demands that any novel catalytic material possessing distinctive activity/selectivity characteristics be stringently investigated, aiding the understanding and promoting the judicious design of more efficient catalysts.[1−3] In order to reach this goal, detailed knowledge of the precise nature and behavior of catalytically active sites at the molecular level is of fundamental importance. A meticulous understanding of structure−property relationships between such sites and the surrounding matrix is also necessary before such a catalyst can be rationally designed.[4] In the vast majority of heterogeneous catalysts, such tempting notions are far from trivial, owing to the difficulties in precise active-site placement, combined with the need for more advanced in situ techniques to specifically probe and engineer active surface sites, which may constitute only a small fraction of the whole system.[5] Single-site heterogeneous catalysts (SSHCs), such as microporous zeotypic solids, where the active sites are in a uniform crystalline environment that is well-distributed throughout the material, are potentially well-suited to overcome some of the above limitations.

Recent research has witnessed widespread developments in the field of multimetallic zeotype catalysts, with a large proportion exploiting the idea of catalytic synergy. A number of examples exist in the literature whereby the combination of two metal dopants results in a favorable modification of the catalytic profile, highlighting potential benefits for the industrial applicability of such designed materials.[6−8] While the notion is undoubtedly appealing, the inclusion of a second metal introduces a further level of complexity that demands a more stringent control from a synthetic perspective. A more detailed knowledge of the local structural environment and associated structure−property relationships is required, not just between the host and the dopants but also between the different heteroatom substituents themselves. To quantify such interactions at the molecular level requires a detailed understanding of the nature of the active sites, and it is necessary to employ a range of physicochemical, operando, and spectroscopic characterization techniques, which are best complemented when integrated with atomic-level modeling studies.[9−15]

In our recent work,[16] we extended the family of transition-metal-doped aluminophosphate (AlPO) frameworks[10,17,18] to

Received: April 10, 2015
Published: June 15, 2015

DOI: 10.1021/jacs.5b03734
J. Am. Chem. Soc. 2015, 137, 8534−8540

obtain isomorphous incorporation of bimetallic active centers that display superior catalytic activity in oxidation reactions (Figure S1 and Table S1, Supporting Information).[16] Through a rational selection of appropriate metal combinations and synthetic strategy, it is possible to engineer and exploit synergic interactions between individual metal sites, deliberately placed within sufficiently close proximity such that their local geometry and electronic structure is modified to facilitate catalytic improvements. It is possible to engineer this phenomenon not only between different dopants but also for different industrially relevant catalytic transformations.[9,16,19−21]

In this paper, we discuss the synergic effects obtained by isomorphously substituting cobalt and titanium ions simultaneously into the same AlPO-5 framework to yield a bimetallic CoTiAlPO-5 system. We have previously shown that individually these two metal dopants (as monometallic entities) are capable of catalyzing a range of oxidation reactions.[22,23] However, we have recently demonstrated[9,16] that their simultaneous incorporation has the potential to induce catalytic synergy. Comprehensive UV/vis studies demonstrated that the local environment around the titanium becomes more tetrahedral when cobalt is present in the same framework.[16] The bimetallic catalyst facilitates more efficient oxidant-activation, increasing product yields. We now present a comprehensive electronic-structure DFT calculation and complementary in situ extended X-ray absorption fine structure (EXAFS) spectroscopy study to elucidate the nature of the active cobalt site within the bimetallic CoTiAlPO-5 catalyst. We contrast the behavior of the monometallic CoAlPO-5 and bimetallic CoTiAlPO-5 active species to uncover the nature of the observed catalytic synergy. Specific emphasis is placed on the cobalt site to provide complementary data to previous findings on the local environment of the titanium ions. By contrasting their behavior in sustainable catalytic applications, we will now demonstrate the benefits of simultaneous incorporation of these two ions.[21]

RESULTS AND DISCUSSION

Cobalt K-edge EXAFS spectra were collected and analyzed to determine the local coordination environment of the active Co site in the calcined (catalytically active) and reduced states (Figure 1 and Figures S2 and S3, Supporting Information). It is known from previous studies that not all the cobalt sites in AlPO-5 framework can be raised to the trivalent oxidation state; therefore, a mixture of environments is expected. All four experimental EXAFS data sets corresponding to oxidized and reduced samples of the mono- and bimetallic catalysts were modeled simultaneously using a similar set of parameters (Table S2). This model includes an oxygen shell and two phosphorus shells for the monometallic catalyst and a Ti shell substituted for one P shell for the bimetallic catalyst (Figures S4 and S5).

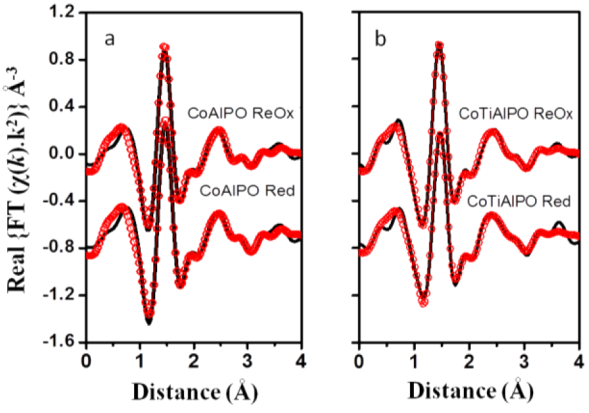

Figure 1. EXAFS data (black) and model (red with symbols) for oxidized (-Reox) and reduced (-Red) monatomic CoAlPO (left) and bimetallic CoTiAlPO (right) samples, showing the real part of the Fourier transform.

In both the monometallic (CoAlPO-5) and bimetallic (CoTiAlPO-5) catalysts, the XANES (Figure S2) and EXAFS data indicate that cobalt is present in four-coordinate geometry, given that the EXAFS coordination number for Co−O shell is approximately 4 (Table 1), as expected for dopants undergoing type I substitution (isomorphous incorporation into the AlPO framework, substituting an Al^{3+} ion). These findings are in excellent agreement with previous UV/vis data on the system, which also confirms that the cobalt ions occupy a tetrahedral geometry (Figure S6).[16] Both the oxidized and reduced monometallic CoAlPO-5 samples showed the possibility of mixed Co environments, as expected, due to the two oxidation states. The EXAFS model indicates the average Co−O bond length of 1.93 ± 0.01 Å for the oxidized catalyst, indicating a mixture of Co^{2+} and Co^{3+}, while the reduced sample shows an extended Co−O bond length of 1.95 ± 0.01 Å, indicating a greater fraction of Co^{2+}ions, in line with previous UV/vis data (Figure S6).[16] The σ^2 factor (0.008 ± 0.001 Å^2) in the first shell Co−O indicates structural disorder, consistent with the mixed oxidation state environment.

In addition to the EXAFS modeling of the first shell, the second shell in the EXAFS spectra can be represented by the split Co−P distance grouped at ∼3.15 and ∼3.4 Å as predicted by the AlPO structure and DFT (Table 2). Indeed, the existence of a next nearest neighbor peak at this distance corresponds well to published literature data for the Co−P distances of the second coordination sphere[22] and is therefore consistent with framework incorporation at Al sites. The lack of appropriate contributions from Co−Co scattering path lengths (which would be expected to occur in the range of 2.9−3.3 Å for cobalt in an oxidic system) shows that the cobalt is isolated within the framework and has not formed metal oxide clusters. The presence of ∼3.0 ± 1.0 P atoms at 3.16 Å, shown by the EXAFS model (Table 1), is in agreement with the DFT calculation for the AlPO structure predicting 3 P atoms between 3.09 and 3.19 Å (see below). The spread in the bond distance of these P atoms results in a relatively large σ^2 value for P. At 3.4 Å, the EXAFS should ideally show 1 P atom but due to the presence of strong multiple scattering signals from mixed Co^{2+} and Co^{3+} environments (between 3.2 and 3.5 Å) the EXAFS analysis is more complex in this region. Our modeling considers the inclusion of only single scattering signals (to reduce the added complexities often associated with the inclusion of multiple scattering signals) and results in ∼2.5 ± 1.0 P atoms at 3.42 Å (Table 1). Consequently, the CN and the associated uncertainty for the second P atom are higher than expected. The bimetallic catalyst spectra were modeled both by replacing the second Co−P scattering path with a Co−Ti path (Table 1) and also with the split P model (Table S3). While the models are statistically similar, the EXAFS data are consistent with the presence of a Co−Ti path in the bimetallic catalyst, and this is strongly supported by the DFT calculations detailed below. This finding supports the notion of adjacent bimetallic substitution, whereby cobalt has undergone a type I

DOI: 10.1021/jacs.5b03734
J. Am. Chem. Soc. 2015, 137, 8534−8540

Table 1. EXAFS Parameters for Monometallic CoAlPO-5 and Bimetallic CoTiAlPO-5 Catalyst Samples

	oxidized			reduced		
path	CN	R (Å)	σ^2 ($\times 10^{-3}$ Å^2)	CN	R (Å)	σ^2 ($\times 10^{-3}$ Å^2)
			Monometallic CoAlPO-5			
Co−O1	3.7 ± 0.2	1.93 ± 0.01	8.1 ± 0.8	4.1 ± 0.2	1.95 ± 0.01	8.1 ± 0.8
Co−P1	2.7 ± 0.9	3.16 ± 0.02	13.4 ± 4.9	2.9 ± 1.0	3.16 ± 0.02	13.4 ± 4.9
Co−P2	1.6 ± 0.7	3.42 ± 0.01	13.4 ± 4.9	2.4 ± 0.9	3.42 ± 0.02	13.4 ± 4.9
			Bimetallic CoTiAlPO-5			
Co−O1	3.8 ± 0.2	1.93 ± 0.01	8.1 ± 0.8	3.5 ± 0.3	1.95 ± 0.01	8.1 ± 0.8
Co−P1	4.0 ± 1.3	3.16 ± 0.02	13.4 ± 4.9	4.1 ± 1.9	3.16 ± 0.02	13.4 ± 4.9
Co−Ti	2.5 ± 1.0	3.24 ± 0.02	13.4 ± 4.9	2.7 ± 1.7	3.24 ± 0.02	13.4 ± 4.9

Table 2. Comparison of Calculated and Experimental Co−O Bond Lengths

Monometallic CoAlPO-5 Distances (Å)			
DFT Co^{II}−O	1.94	DFT Co^{III}−O	1.82
EXAFS reduced Co−O	1.95	EXAFS oxidized Co−O	1.93
Bimetallic CoTiAlPO-5 Distances (Å)			
DFT Co^{II}−O	1.92	DFT Co^{III}−O	1.82
EXAFS reduced Co−O	1.95	EXAFS oxidized Co−O	1.93

substitution mechanism (substituting Al^{3+}), while simultaneously titanium has undergone a type II substitution (isomorphous substitution into the AlPO framework to replace a P^{5+} ion), adjacent to the cobalt. This dopant cluster may modify the local structural strain relative to isolated dopant sites, leading to a different local environment of Co.

The ability of cobalt to undergo type I substitution (replacing Al^{3+}, as determined from the EXAFS results) and titanium to undergo type II substitution (replacing P^{5+}) was used as the basis to probe the active site(s) directly using computational chemistry methods. The lowest energy geometries of monometallic (Co^{2+}, Co^{3+}, and Ti^{4+}) and undoped AlPO-5 systems were calculated using periodic DFT calculations; full structural results are reported in the ESI. The structure of undoped AlPO-5, with lattice parameters $a = b = 13.75$ Å, $c = 8.35$ Å, and individual Al−O and P−O bond lengths of 1.74 ± 0.02 and 1.54 ± 0.01 Å, is in good agreement with literature values (Tables S4 and S5).[22,24] On isomorphously substituting a Co^{2+} ion for Al^{3+} (and introducing the appropriate charge-balancing proton), both the high-spin and low-spin d^7 electronic configurations were investigated. The high-spin state was found to be the stable electronic state, as expected for a first-row transition element four coordinated by electron-donor ligands. Incorporation of Co^{2+} causes a local structural expansion relative to Al; the equilibrium structure contains three Co−O bonds of ∼1.88 Å (1.87, 1.88, and 1.90 Å) and a significantly longer Co−OH bond to the protonated framework oxygen (2.12 Å, Tables S6 and S7). An elongation of 0.1 Å or more of the bond distances between framework ions and protonated relative to nonprotonated oxygen ions is invariably observed in all doped zeotypes.[24]

The oxidized Co^{3+} ion in a framework Al site is again stable in high-spin (d^6) electronic configuration. Its calculated equilibrium bond distances (Table S8) are shorter and more symmetric than those of Co^{2+} due to the smaller ionic radius of Co^{3+} relative to Co^{2+} and the absence of protonated oxygens in the first coordination shell of Co^{3+}. The Co−O distances calculated for the monometallic CoAlPO-5 systems, averaged over the 4 nearest neighbor oxygens of Co, are 1.94 and 1.82 Å for Co^{2+} and Co^{3+}, respectively, in agreement with the experimental EXAFS results (Table 1). The equilibrium Co−P distances in the second coordination shell of Co range between 3.096 and 3.196 Å, also in good agreement with those found experimentally from the EXAFS modeling (3.16 Å), confirming that type I substitution (Co^{2+} replacing a framework Al^{3+}) has occurred. Given the agreement of calculated and observed geometries, it follows that our computational model is appropriate for a quantitative description of the cobalt sites found experimentally.

In both Co^{2+} and Co^{3+} systems, the oxygen ions nearest neighbor of Co show a small spin polarization (see Tables S7 and S9), obtained by π donation from the oxide ions into the singly occupied d atomic orbitals of Co. The donation is higher for Co^{3+}, given its stronger Lewis acid character, resulting in a higher spin polarization (of ∼0.2|e|) on the oxygen ions bonded to Co^{3+} than those bonded to Co^{2+} (0.08|e|). Hydrocarbon oxidation reactions in metal-doped AlPOs initiate through a homolytic H-abstraction step from a framework O next to the dopant.[25−27] Increased spin polarization on this oxygen facilitates the radical mechanism and therefore correlates with catalytic activity.

The monometallic Ti^{4+}AlPO-5 system was simulated by replacing a framework P^{5+} ion with Ti^{4+}, through type II substitution, in agreement with our previous UV/vis data (Figure S6B). The equilibrium structure around Ti consists of three shorter Ti−O bonds (1.75, 1.77, and 1.78 Å, Table S10), while the protonated Ti−OH bond again shows a significant expansion (1.99 Å, Table S10). It is important to note that Ti causes a significant expansion relative to the framework P ion it replaces (whose P−O bond distances are of 1.54 Å). The electronic structure of Ti^{4+}AlPO-5 reveals no spin polarization, consistent with the d^0 configuration of Ti^{4+} (Table S11).

Having characterized computationally the local environment of Co and Ti in the monometallic Me-AlPO-5 systems, we now discuss our findings when one Co (in either +2 or +3 oxidation state) and one Ti^{4+} ion are simultaneously incorporated in the same AFI unit cell. Apart from quantitatively interpreting the EXAFS results, our goal was also to identify similarities and differences in the geometry and electronic structure of mono- and bimetallic materials, which can provide valuable insights into the synergic catalytic enhancement observed experimentally.[9,16] The first feature we have investigated is the configurational landscape of the codoped material, i.e., the relative stability of Co and Ti ions located at different separation in the framework. The configurations examined include Co and Ti in nearest neighbor (adjacent) T sites and further apart in the structure (Table S12). In these initial calculations, cobalt was purposefully limited to the divalent "as-

DOI: 10.1021/jacs.5b03734
J. Am. Chem. Soc. 2015, 137, 8534−8540

synthesized" state to represent the ions during the crystallization stage, as this is the point at which the dopant location in the framework is determined. The relative stability of different (Co, Ti) configurations in the bimetallic catalyst is related to the energy of separated Co and Ti sites in the monometallic solids through the definition of a clustering energy (E_{clu}) given by eq 1

$$E_{clu} = E[Co^{2+}Ti^{4+}AlPO\text{-}5] + E[AlPO\text{-}5] - E[Co^{2+}AlPO\text{-}5] - E[Ti^{4+}AlPO\text{-}5] \quad (1)$$

where E[M(M′)AlPO-5] are the calculated energies of one AlPO-5 unit cell containing the M (and M′) dopants and E[AlPO-5] is the energy of one undoped unit cell. Negative clustering energies indicate stability of the bimetallic system relative to separate monometallic ones.

Co^{2+} and Ti^{4+} ions each require one proton for charge balance. Binding one proton to one of the four nearest neighbor oxygens of both ions gives rise to 16 distinct proton distributions; all 16 have been examined explicitly for Co−Ti in adjacent T sites (Table S13) and further apart in the same unit cell of AlPO-5 (Table S14). The choice of protonation sites is critical, especially for the case of Co−Ti clustered in nearest T sites, where it accounts for a variation of over 136 kJ/mol in the energy (Table S13). It is therefore essential to examine exhaustively the possible protonation sites. For each (Co, Ti) configuration, the results in Table S12 are based on the most stable proton distribution. Clustering energies of Co^{2+} and Ti^{4+} are calculated to be negative for all bimetallic cells investigated, and there is a clear trend between proximity of Co to Ti and stability. The most stable configuration corresponds to Co and Ti in adjacent T sites, with clustering energy of −66.6 kJ/mol; Co and Ti in the next nearest T site configuration (i.e., forming a Co−P−Al−Ti unit) have instead a calculated clustering energy of −22.8 kJ/mol.

These results clearly indicate a thermodynamic preference for Co and Ti to be located in close proximity in the bimetallic catalyst and, in particular, for adjacent bimetallic substitution of the two elements. During synthesis the likelihood of Co−O−Ti units forming is improved; thus, we can expect a larger fraction of Co and Ti sites to be located in close proximity. This result further validates the EXAFS model used which includes a Co−Ti path in the bimetallic catalyst which provides an atomic structure link to the observed catalytic synergy.

Analysis of the Co−O bond distances in the equilibrium structure calculated for adjacent Co−Ti sites in the bimetallic solid (Figure 2 and Tables S15 and S17) shows a subtly different structural environment than in the monometallic CoAlPO-5. In particular, the bridging oxygen between Co and Ti ions has much shorter Co−O bond distance (1.97 vs 2.12 Å). We attribute this feature to the larger ionic radius of Ti^{4+} relative to P^{5+}, which can be equated to a local chemical pressure that compresses the adjacent Co−O(H) bond. When averaged over all four nearest neighbor oxygens, the EXAFS model showed both were 1.93 ± 0.01 Å. However, this average value may not be a significant parameter for the bimetallic solid, given the significant spread among the individual bond distances. When considering Co and Ti dopants in the same unit cell, but in nonadjacent T sites (Tables S19 and S21), we observe a local structure for Co^{2+} where three Co−O bonds are slightly longer than in the monometallic solid and one considerably shorter, resulting in values averaged over the four nearest neighbors of 1.94 Å, the same as in the monometallic solid.

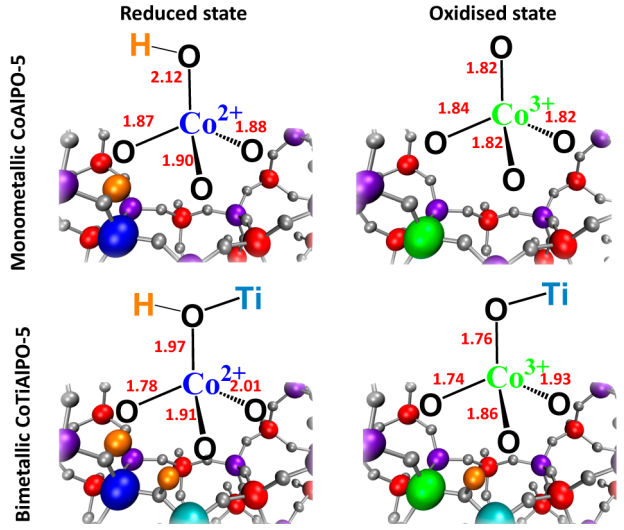

Figure 2. Calculated equilibrium bond distances for mono- and bimetallic, oxidized, and reduced cobalt sites.

The fact that Co and Ti are most stable when in adjacent framework T sites deserves a more in-depth analysis. Both Co^{2+} and Ti^{4+} dopant ions require a lattice expansion relative to the undoped framework; hence, clustering generates a buildup of steric strain, as demonstrated by the bond distances discussed above. Comparing the equilibrium structure around Co, it is evident that the chemical pressure generated by Ti in the local environment causes a substantial compression of the bridging Co−O bond. A possible rationale to explain the favorable clustering originates from the unique properties of the O ion bridging Co and Ti dopants in adjacent T sites. Analysis of calculated charges shows that this bridging oxygen is much more basic and more ionic than the oxygens directly bonded to P. The latter form acidic molecular orthophosphate (PO_4^{3-}) ions in AlPOs. The basicity of the Co−Ti bridging oxygen results in a more favorable protonation energy and the ionicity in enhanced structural flexibility due to nondirectional ionic bonding. The latter feature is demonstrated by the equilibrium Co−O−Ti angle of 111.68°, which is much smaller than the Al−O−P angle (140.95°) in the undoped framework but also smaller than Co−O−P (133.85°) and Al−O−Ti (130.17°) angles in the monometallic catalysts. The Co−O−P angle for Co near but not adjacent to Ti in the bimetallic solid has an intermediate value of 126.30°. The increased flexibility of the Co−O−Ti angle in the bimetallic catalyst contributes to absorb the steric strain caused by doping, hence stabilizing the dopant clustering.

It is finally important to stress that all calculations reported in this study on the reduced bimetallic materials converged to the $Co^{2+}Ti^{4+}$ electronic state and, despite attempts to appropriately constrain the spin, we did not observe any evidence (under our conditions) for the existence of the isoelectronic $Co^{3+}Ti^{3+}$structure. Cobalt is therefore the redox-active ion in the bimetallic catalyst, while Ti serves the major goal of providing synergic activation of Co while remaining itself in the 4+ oxidation state throughout.

In order to draw meaningful comparisons with the behavior of the monometallic species, equilibrium geometry and energy of the oxidized bimetallic $Co^{3+}Ti^{4+}$AlPO-5 catalyst were also

DOI: 10.1021/jacs.5b03734
J. Am. Chem. Soc. 2015, 137, 8534−8540

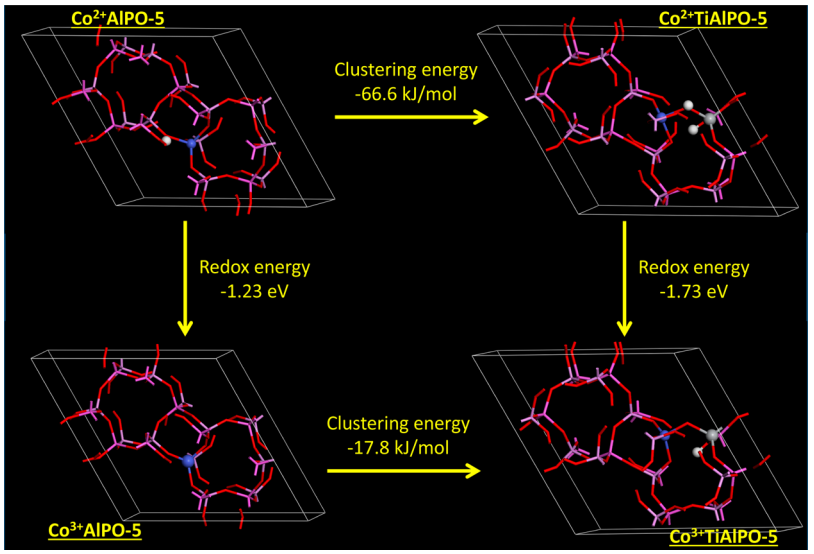

Figure 3. Reduction energy of Co^{3+} with molecular hydrogen in monometallic and bimetallic materials.

calculated. We first consider the material containing the stable Co−O−Ti bridge. The geometries were derived from that of $Co^{2+}Ti^{4+}$AlPO-5 by removing either of the two protons. The lowest energy configuration retained the proton associated with the titanium ion only, via loss of the proton bound to the oxygen of the Co−O−Ti bridge. The system with Co^{3+} and Ti^{4+} ions in adjacent T sites has a calculated clustering energy of −17.9 kJ/mol relative to isolated dopant ions, while Co^{3+} and Ti^{4+} ions in the same unit cell but nonadjacent have a calculated clustering energy of −8.3 kJ/mol. Also in the 3+ oxidation state, therefore, Co is stable when in proximity of Ti, although clustering energies are substantially smaller than for Co^{2+}.

As for Co^{2+}, the bridging oxygen between Co^{3+} and Ti ions has much shorter Co−O bond distances than in the monometallic Co-AlPO-5 material (1.76 vs 1.82 Å see Figure 2) due to the ionic size of the Ti (Table 2). This is accompanied by a longer (1.93 Å) Co−O bond, so that the average over all four nearest neighbor oxygens is of 1.82 Å, unchanged relative to the monometallic solid. When considering Co and Ti in nonadjacent T sites (Table S21), we observe a local structure where three Co−O bonds are slightly longer than in the monometallic solid and one is considerably shorter, resulting in values averaged over the four nearest neighbors of 1.82 Å, again the same as in the monometallic solid (Table 2).

The calculated energies for the mono- and bimetallic materials in oxidized and reduced forms can be combined to evaluate the reduction energy (+3/+2) of Co in the catalysts via eq 2 and 3

$$\Delta E = E[\mathrm{Co^{2+}AlPO\text{-}5}] - E[\mathrm{Co^{3+}AlPO\text{-}5}] - E[\mathrm{H_2}]/2 \quad (2)$$

$$\Delta E = E[\mathrm{Co^{2+}Ti^{4+}AlPO\text{-}5}] - E[\mathrm{Co^{3+}Ti^{4+}AlPO\text{-}5}] - E[\mathrm{H_2}]/2 \quad (3)$$

where $E[H_2]$ is the energy of a gas-phase hydrogen molecule calculated consistently with that of the solid catalysts. ΔE is intrinsically linked to the catalytic activity of MeAlPOs in selective oxidation reactions, where the reduction of the metal from +3 to +2 occurs in the rate-limiting steps.[25,26]

The reduction energy of Co in the monometallic CoAlPO-5 material is calculated to be −1.23 eV/ion, corresponding to a standard reduction potential of 1.23 V (Figure 3). This value is lower than other cobalt-substituted AlPO materials,[24] indicating greater preference for the divalent over the trivalent state, and in good agreement with previous studies that showed the redox fraction in CoAlPO-5 to be lower than in most other AlPO structures.[22] The equivalent reduction energy is −1.73 eV/ion for Co adjacent to Ti in the bimetallic CoTiAlPO-5 system (Figure 3). The bimetallic species favors therefore the divalent state to a greater extent than the monometallic system and may thus be expected to be more catalytically active. By contrasting the calculated clustering energies for +2 and +3 oxidation states of cobalt in mono- and bimetallic solids, we conclude that the higher reduction potential of Co is to be attributed to a higher stabilization of the divalent state relative to the trivalent in the bimetallic solid, resulting in favorable reduction.

It is important to note at this stage that despite the higher reduction potential, a fraction of cobalt is still raised to the Co^{3+} state during calcination in the bimetallic solid, accounting for the color change from blue (precalcinaton) to green (postcalcination).

It is not only the geometry but also the electronic structure of the oxygen ion bridging adjacent Co and Ti ions that is substantially different from the monometallic systems. The spin polarization of this oxygen in the oxidized catalyst, of 0.419|e| (Table S18), is much higher than in the monometallic solid (0.218 |e|, Table S8). The spin polarization is highlighted in Figure 4. The unique environment of the bridging oxygen directly bonded to two transition-metal ions enables effective spin delocalization from Co^{3+} to Ti^{4+} through superexchange interaction, the mechanism responsible for magnetic coupling in transition metal oxides, but unavailable for main group elements. Since selective oxidation reactions in metal-doped AlPOs proceed via radical abstractions of hydrogen atoms from the hydrocarbon substrates,[25,26] it is not unreasonable to expect the spin polarization of the bridging oxygen to be associated with higher activity, given the increased stabilization of the oxidized trivalent state, relative to the reduced divalent state. The transition between which is fundamental to the activity of these materials. If the correlation between spin polarization and

DOI: 10.1021/jacs.5b03734
J. Am. Chem. Soc. 2015, 137, 8534−8540

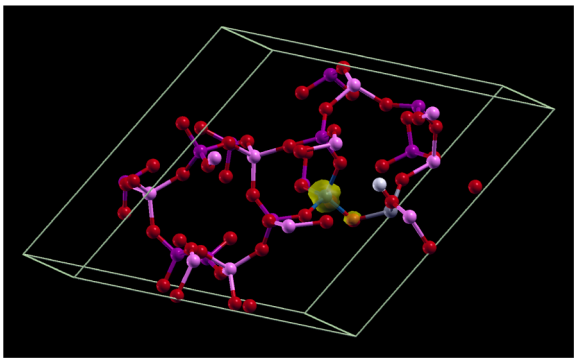

Figure 4. Spin density plot of $Co^{3+}Ti^{4+}$AlPO-5, containing adjacent Co(blue) and Ti(gray) ions, highlighting the high spin polarization of the Co−O−Ti bridging oxygen.

activity could be confirmed in a broader range of bimetallic solids, we would have identified a molecular descriptor able to represent catalytic activity, suitable for rational computational screening of new catalysts.

CONCLUSION

In summary, we have explored the synergic catalytic enhancement displayed by the bimetallic CoTiAlPO-5 system, in sustainable oxidation reactions, with particular emphasis on the isomorphously substituted, tetrahedral $Co^{2+/3+}$ active site, and its implicit role in the catalytic process. Co is the redox-active ion in the bimetallic catalyst, with Ti providing synergic activation, while remaining itself in +4 oxidation state throughout. The synergistic catalytic enhancement of the bimetallic system can be explained on the basis of the thermodynamic stability of the Co and Ti ions toward clustering, which leads to a significant amount of Co and Ti ions being located in adjacent T sites, as evidenced through both computational chemistry and experimental spectroscopic findings. This adjacent substitution forces subtle changes in the local structural environment and electronic structure of the cobalt site, which translate into significant modifications of the redox behavior, which is crucial for enhanced catalytic performance in selective oxidation reactions. We have further demonstrated that the stability of cobalt in its divalent oxidation state is further augmented in the bimetallic catalyst, prompting a more energetically favorable rate-determining step in the oxidation reactions, which can help explain the observed synergies in catalytic performance.

EXPERIMENTAL SECTION

EXAFS Modeling. The EXAFS spectra were modeled using ARTEMIS[28] and FEFF6.0[29] for the theoretical calculations based on crystal structures obtained by DFT calculations in this study. For monometallic CoAlPO, the EXAFS models include single scattering O paths with Co−O distances of 1.87 Å and two single scattering P path with Co−P distance of 3.1 and 3.4 Å. For bimetallic CoTiAlPO, the EXAFS model replaced one Co−P signal with a scattering path from Ti with a distance from Co of around 3.26 Å (resulting from a Co−O−Ti entity). There are 11 parameters used to describe the monometallic and bimetallic models listed in Table 1: four coordination numbers (CN), four changes in path length (ΔR), two mean square displacements of the half-path length values (σ^2), and an energy shift parameter (ΔE). The value for S_0^2 (0.82 ± 0.05) was determined from Co foil. The data range from 2.5 to 9.5 $Å^{-1}$ was used in the Fourier transform (FT) with *k*-weights of 1 and 2. The model was applied to the FT range of 1.0 to 3.5 Å. The EXAFS data and model are shown in Figure S4. All four data sets were modeled simultaneously. This dramatically increases the information content in the data to 40 independent points and 20 parameters.

Computational Details. Electronic structure calculations were performed on the University of Southampton Iridis3 supercluster with the CRYSTAL09 periodic DFT code using the B3LYP hybrid-exchange functional.[30−34] The AFI framework was calculated using periodic boundary conditions in *P*1 space group to allow full-optimization without symmetry constraints. The electronic distribution was described as a linear combination of atomic orbitals and the basis functions are expressed as Gaussian-type orbitals. Aluminum, phosphorus, oxygen, and hydrogen ions were described using a double-valence plus polarization basis set whereas titanium and cobalt were described using a triple-valence plus polarization basis set. All basis sets employed were taken from the online library for the CRYSTAL code.[35] The AFI structure was described by modeling one unit cell containing 72 atoms (12 $AlPO_4$ formula units). Cobalt was substituted for aluminum and titanium was substituted for phosphorus. In the case of a charge imbalance (Co^{2+} substituting Al^{3+} or Ti^{4+} substituting for P^{5+}), a proton was attached to an oxygen ion adjacent to the divalent or tetravalent dopant. One substitution was made per metal per unit cell, corresponding to 8.3 mol % loading.

ASSOCIATED CONTENT

Supporting Information

Additional experimental, computational, mechanistic, and catalytic data. The Supporting Information is available free of charge on the ACS Publications website at DOI: 10.1021/jacs.5b03734.

AUTHOR INFORMATION

Corresponding Authors

*matthew.potter@chbe.gatech.edu
*r.raja@soton.ac.uk

Notes

The authors declare no competing financial interest.

ACKNOWLEDGMENTS

We acknowledge Honeywell LLC for financial support. Use of the Advanced Photon Source, an Office of Science User Facility operated for the U.S. Department of Energy (DOE) Office of Science by Argonne National Laboratory, was supported by the U.S. DOE under Contract No. DE-AC02-06CH11357. MRCAT operations are supported by the Department of Energy and the MRCAT member institutions.

REFERENCES

(1) Maschmeyer, T.; Rey, F.; Sankar, G.; Thomas, J. M. *Nature* **1995**, *378*, 159−162.
(2) Bell, A. T. *Science* **2003**, *299*, 1688−1691.
(3) Lee, J.; Farha, O. K.; Roberts, J.; Scheidt, K. A.; Nguyen, S. T.; Hupp, J. T. *Chem. Soc. Rev.* **2009**, *38*, 1450−1459.
(4) Oldroyd, R. D.; Thomas, J. M.; Sankar, G. *Chem. Commun.* **1997**, *21*, 2025−2056.
(5) Corma, A.; Nemeth, L. T.; Renz, M.; Valenica, S. *Nature* **2001**, *412*, 423−425.
(6) Kesavan, L.; Tiruvalam, R.; Ab Rahim, M. H.; bin Saiman, M. I.; Enache, D. I.; Jenkins, R. L.; Dimitratos, N.; Lopez-Sanchez, J. A.; Taylor, S. H.; Knight, D. W.; Kiely, C. J.; Hutchings, G. J. *Science* **2011**, *331*, 195−199.
(7) Hungaria, A. B.; Raja, R.; Adams, R. D.; Captain, B.; Thomas, J. M.; Midgley, P. A.; Golovoko, V.; Johnson, B. F. G. *Angew. Chem., Int. Ed.* **2006**, *45*, 4782−4785.
(8) Gianotti, E.; Manzoli, M.; Potter, M. E.; Shetti, V. N.; Sun, D.; Paterson, A. J.; Mezza, T.; Levy, A. B.; Raja, R. *Chem. Sci.* **2014**, *5*, 1810−1819.

DOI: 10.1021/jacs.5b03734
J. Am. Chem. Soc. 2015, 137, 8534−8540

(9) Leithall, R. M.; Shetti, V. N.; Maurelli, S.; Chiesa, M.; Gianotti, E.; Raja, R. *J. Am. Chem. Soc.* **2013**, *135*, 2915−2918.
(10) Thomas, J. M.; Sankar, G. *Acc. Chem. Res.* **2001**, *34*, 571−581.
(11) O'Brien, M. G.; Beale, A. M.; Jacques, S. D. M.; Di Michiel, M.; Weckhuysen, B. M. *Appl. Catal. A-Gen.* **2011**, *391*, 468−476.
(12) Arean, C. O.; Weckhuysen, B. M.; Zecchina, A. *Phys. Chem. Chem. Phys.* **2012**, *14*, 2125−2127.
(13) Lamberti, C.; Bordiga, S.; Bonino, F.; Prestipino, C.; Berlier, G.; Capello, L.; D'Acapito, F.; Xamena, F. X. L. I.; Zecchina, A. *Phys. Chem. Chem. Phys.* **2003**, *5*, 4502−4509.
(14) Bartlett, S. A.; Wells, P. P.; Nachtegaal, M.; Dent, A. J.; Cibin, G.; Reid, G.; Evans, J.; Tromp, M. *J. Catal.* **2011**, *284*, 247−258.
(15) Gilson, J. P.; Fernandez, C.; Thibault-Starzyk, F. *J. Mol. Catal. A-Chem.* **2009**, *305*, 54−59.
(16) Paterson, A. J.; Potter, M. E.; Gianotti, E.; Raja, R. *Chem. Commun.* **2011**, *47*, 517−519.
(17) Thomas, J. M.; Raja, R.; Lewis, D. W. *Angew. Chem., Int. Ed.* **2005**, *44*, 6456−6482.
(18) Thomas, J. M.; Raja, R. *Annu. Rev. Mater. Res.* **2005**, *35*, 315−350.
(19) Potter, M. E.; Sun, D.; Gianotti, E.; Manzoli, M.; Raja, R. *Phys. Chem. Chem. Phys.* **2013**, *15*, 13288−13295.
(20) Lefenfeld, M.; Raja, R.; Paterson, A. J.; Potter, M. E. US Patent 021882, 2010.
(21) Thomas, J. M.; Raja, R. *Proc. Natl. Acad. Sci. U.S.A.* **2005**, *39*, 13732−13736.
(22) Sankar, G.; Raja, R.; Thomas, J. M. *Catal. Lett.* **1998**, *55*, 15−23.
(23) Lee, S. O.; Raja, R.; Harris, K. D. M.; Thomas, J. M.; Johnson, B. F. G.; Sankar, G. *Angew. Chem., Int. Ed.* **2003**, *115*, 1558−1561.
(24) Cora, F.; Alfredsson, M.; Barker, C. M.; Bell, R. G.; Foster, M. D.; Saadoune, I.; Simplerer, A.; Catlow, C. R. A. *J. Solid State Chem.* **2003**, *176*, 496−529.
(25) Gomez-Hortiguela, L.; Cora, F.; Sankar, G.; Zicovich-Wilson, C. M.; Catlow, C. R. A. *Chem.—Eur. J.* **2010**, *16*, 13638−13645.
(26) Gomez-Hortiguela, L.; Cora, F.; Catlow, C. R. A. *ACS Catal.* **2011**, *1*, 18−28.
(27) Corà, F.; Catlow, C. R. A.; Gómez-Hortigüela, L. *Proc. Roy. Soc. A* **2012**, *468*, 2053−2069.
(28) Ravel, B.; Newville, M. *J. Synchrotron Radiat.* **2005**, *12*, 537−541.
(29) Zabinsky, S. I.; Rehr, J. J.; Ankudinov, A.; Albers, R. C.; Eller, M. J. *J. Phys. Rev. B* **1995**, *52*, 2995.
(30) Dovesi, R.; Orlando, R.; Civalleri, B.; Roetti, C.; Saunders, V. R.; Zicovich-Wilson, C. M. *Z. Kristallogr.* **2005**, *220*, 571−573.
(31) Becke, A. D. *J. Phys. Chem.* **1993**, *98*, 5648−5652.
(32) Lee, C.; Yang, W.; Parr, R. G. *Phys. Rev. B* **1988**, *37*, 785−789.
(33) Vosko, S. H.; Willk, L.; Nusair, M. *Can. J. Phys.* **1980**, *58*, 1200−1211.
(34) Stephens, P. J.; Devlin, F. J.; Chabalowski, C. F.; Frisch, M. J. *J. Phys. Chem.* **1994**, *98*, 11623−11627.
(35) *CRYSTAL Basis Sets Library*, http://www.crystal.unito.it/Basis_Sets/Ptable.html (accessed Nov 2011).

DOI: 10.1021/jacs.5b03734
J. Am. Chem. Soc. 2015, 137, 8534−8540